

Carbon isotope stratigraphy, magnetostratigraphy, and $^{40}\text{Ar}/^{39}\text{Ar}$ age of the Cretaceous South Atlantic coast, Namibe Basin, Angola



Christopher Strganac^{a,b,*}, Johanna Salminen^{c,d}, Louis L. Jacobs^a, Michael J. Polcyn^a, Kurt M. Ferguson^a, Octávio Mateus^{e,f}, Anne S. Schulp^{g,h,i}, Maria Luísa Morais^j, Tatiana da Silva Tavares^{j,k}, António Olímpio Gonçalves^j

^a Roy M. Huffington Department of Earth Sciences, Southern Methodist University, 3225 Daniel Avenue, Dallas, TX 75275, USA

^b Perot Museum of Nature and Science, Dallas, TX 75201, USA

^c Division of Geophysics and Astronomy, Department of Physics, P.O. Box 64, 00014 University of Helsinki, Finland

^d Department of Geosciences and Geography, P.O. Box 64, 00014 University of Helsinki, Finland

^e CICEGe, Faculdade de Ciências e Tecnologia, Universidade Nova de Lisboa, Caparica, Portugal

^f Museu da Lourinhã, Rua João Luis de Moura, 2530-157 Lourinhã, Portugal

^g Naturalis Biodiversity Center, Darwinweg 2, P.O. Box 9517, 2300RA Leiden, The Netherlands

^h Natuurhistorisch Museum Maastricht, De Bosquetplein 6/7, 6211KJ Maastricht, The Netherlands

ⁱ Faculty of Earth and Life Sciences, Vrije Universiteit Amsterdam, De Boelelaan 1085, 1081HV Amsterdam, The Netherlands

^j Departamento de Geologia, Faculdade de Ciências, Universidade Agostinho Neto, Avenida 4 de Fevereiro 7, Luanda, Angola

^k Université de Bourgogne, Dijon, France

ARTICLE INFO

Article history:

Received 30 June 2013

Received in revised form 8 March 2014

Accepted 10 March 2014

Available online 21 March 2014

Keywords:

Cretaceous

Stable carbon isotopes

Chemostratigraphy

Magnetic polarity stratigraphy

Africa

Atlantic

ABSTRACT

We present the $\delta^{13}\text{C}$ and paleomagnetic stratigraphy for marine strata at the coast of southern Angola, anchored by an intercalated basalt with a whole rock $^{40}\text{Ar}/^{39}\text{Ar}$ radiometric age of 84.6 ± 1.5 Ma, being consistent with both invertebrate and vertebrate biostratigraphy. This is the first African stable carbon isotope record correlated to significant events in the global carbon record spanning the Late Cenomanian to Early Maastrichtian. A positive $\sim 3\text{‰}$ excursion seen in bivalve shells below the basalt indicates the Cenomanian–Turonian Boundary Event at 93.9 Ma, during Oceanic Anoxic Event 2. Additional excursions above the basalt are correlated to patterns globally, including a negative $\sim 3\text{‰}$ excursion near the top of the section interpreted as part of the Campanian–Maastrichtian Boundary Events. The age of the basalt ties the studied Bentiaba section to a pulse of Late Cretaceous magmatic activity around the South Atlantic and significant tectonic activity, including rotation, of the African continent.

© 2014 The Authors. Published by Elsevier Ltd. This is an open access article under the CC BY-NC-SA license (<http://creativecommons.org/licenses/by-nc-sa/3.0/>).

1. Introduction

The separation of South America and Africa was one of the most significant global tectonic episodes during the Mesozoic, representing the last major division of Gondwana that led to the formation of the South Atlantic Ocean. This paper focuses on the chronology of coastal Angola during the Late Cretaceous, after the Early Cretaceous opening of the South Atlantic, as the ocean grew significantly. We utilize the widespread South Atlantic magmatic event to anchor a new southern hemisphere $\delta^{13}\text{C}$ curve and a magnetostratigraphic section encompassing most of the Late Cretaceous period.

Coastal outcrops of the Namibe Basin (Fig. 1) contain Cretaceous volcanics, non-marine synrift sediments, and marine post-rift

sediments deposited along the uplifted pre-Mesozoic basement that forms part of the structural margin of the South Atlantic (Burke and Gunnell, 2008). The location of southern Angola at the northern extent of the Namib Desert allows examination of the geological history of the region unimpeded by dense vegetation, including the Late Cretaceous marine transgression of the coast. The most recent previous fieldwork that extensively examined the onshore geology of Angola was published in the 1960s (Carvalho, 1961; Antunes, 1964), i.e., prior to widespread acceptance of plate tectonics, advances in methods of radiometric dating, development of the paleomagnetic time scale, or stable carbon isotope stratigraphy. In this paper, we present the stable carbon isotope chemostratigraphy derived from bivalve shells and the magnetostratigraphy at Bentiaba, Namibe Basin, Angola. The proposed stratigraphy is calibrated by a radiometric age on an intercalated basalt and correlated to the astronomically tuned magnetostratigraphic time scale and to global Cretaceous marine

* Corresponding author. Tel.: +1 214 756 5829.

E-mail address: christopher.strganac@perotmuseum.org (C. Strganac).

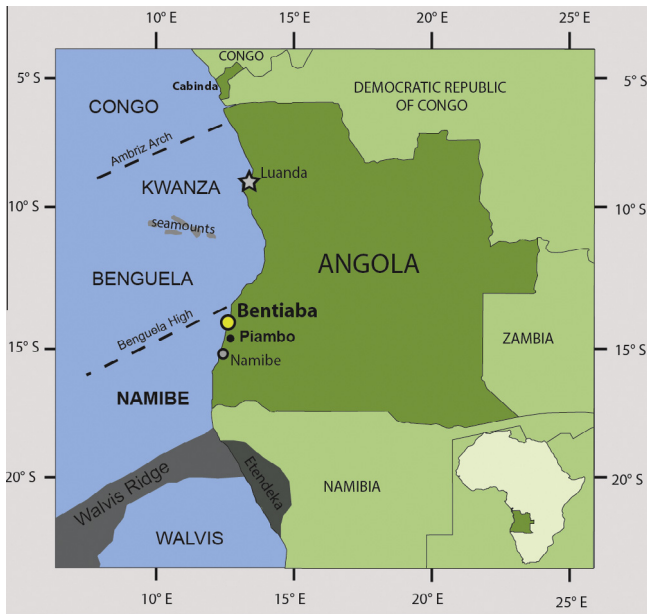


Fig. 1. Location map of Bentiaba. Inset in lower right shows location of Angola in Africa. Offshore basins (such as Kwanza) are labeled in upper case. Darker shaded regions are the primary extent of Etendeka LIP and Walvis Ridge (modified from Comin-Chiaramonti et al., 2011).

carbon isotope curves. These correlations are consistent with both invertebrate and vertebrate biostratigraphy at Bentiaba. This is the first chemo- and magnetostratigraphic study of its kind along the African South Atlantic.

1.1. Background

Torsvik et al. (2009) reviewed the rifting and subsequent drifting apart of South America and Africa and presented a new geophysical model for the origin of the South Atlantic Ocean. Two magmatic pulses were identified around the South Atlantic during the Cretaceous, flood basalts of the Paraná–Etendeka large igneous province, which erupted between 137 to 127 Ma, and younger alkaline to transitional magmatism, which peaked around 83.5 Ma (Torsvik et al., 2009). In Angola, Marzoli et al. (1999) identified tholeiitic basalts, about 131 Ma, that correlate in age and composition to flood basalts at Etendeka, Namibia. In Angola's Kwanza and Benguela basins, north of the study area, younger magmatism is represented by alkaline and transitional basalts intercalated within Late Cretaceous marine sediments (Marzoli et al., 1999; Comin-Chiaramonti et al., 2011). Radiometric ages of 91 ± 2 and 93 Ma were reported for the alkaline basalt flows in the Kwanza Basin (Marzoli et al., 1999; Comin-Chiaramonti et al., 2011).

In the Namibe Basin, two stratigraphically distinct volcanic episodes are present in the Cretaceous sequence. Both units crop out at Piambo and are separated stratigraphically by synrift gypsum deposits and conglomerates. Near Bentiaba, about 50 km north of Piambo, the Ombe Formation is a basalt flow that intercalates with Late Cretaceous marine sediments unconformably overlying synrift redbeds. The sequence is part of the São Nicolau Group (Cooper, 1976, 2003a). Cooper (1976, 2003a,b) biostratigraphically assigned ammonite faunas from strata subjacent to the basalt to Turonian and Lower Coniacian and he assigned strata superjacent to the basalt to the Middle Santonian, which posited an age for the basalt between 89 and 85 Ma. Thus, the basalt would correspond to Middle Coniacian to Lower Santonian age, placing the flow in the

younger magmatic pulse of the South Atlantic (Cooper, 2003b; Torsvik et al., 2009).

1.2. Cretaceous carbon isotope events

The potential of using stable carbon isotopes to correlate sections globally was demonstrated by Scholle and Arthur (1980) by comparing patterns in bulk carbonate $\delta^{13}\text{C}$ from Late Cretaceous localities along the Atlantic including the English Chalk of the Boreal Chalk Sea, the Mediterranean at Gubbio, Italy, and the Cretaceous–Paleogene Boundary at DSDP Site 356 on the Walvis Ridge. Correlation of carbon isotope curves is possible because large-scale perturbations in the global carbon cycle are reflected in the $\delta^{13}\text{C}$ of marine carbonate. In the Late Cretaceous, the largest recorded event is a positive excursion at the Cenomanian–Turonian boundary that reflects Oceanic Anoxic Event 2, a widely recognized period of increased burial of organic carbon (Schlanger and Jenkyns, 1976; Scholle and Arthur, 1980; Schlanger et al., 1987; Arthur et al., 1988; Jarvis et al., 2006).

Jarvis et al. (2006) refined the Cenomanian to Late Campanian $\delta^{13}\text{C}$ stratigraphy of the English Chalk, and correlated the resulting pattern to sections in France, Germany, Spain, and Italy. The correlations generally agreed with biostratigraphic correlations, but the chemostratigraphy proved a more accurate method of correlating between Boreal and Tethyan regions than nannofossil biostratigraphy (Jarvis et al., 2006). Voigt et al. (2010, 2012) and Thibault et al. (2012a,b) presented high-resolution Late Campanian–Maastrichtian carbon isotope values from the Boreal Chalk Sea, the Pacific and Indian Oceans, and the Tethys that allowed global correlation.

Carbon isotope studies at DSDP Sites 530A and 525A adjacent to the Namibe Basin on the Walvis Ridge produced patterns identified as the Cenomanian–Turonian Boundary Event and the Campanian–Maastrichtian Boundary Events, respectively, and are the current references used to correlate the South Atlantic globally during the Late Cretaceous (Li and Keller, 1999; Forster et al., 2008; Voigt et al., 2012). While the Walvis Ridge drill core sites record high-resolution $\delta^{13}\text{C}$ change, the curves are limited temporally to the Late Cenomanian–Early Turonian and Late Campanian–Early Paleogene intervals.

Biostratigraphic correlations indicate a Late Cenomanian to Maastrichtian age for deposition of the marine strata at Bentiaba. An ammonite fauna near the base of the marine section was correlated with the Late Cenomanian *Sciponoceras gracile* Zone in North America and the float recovery of *Watinoceras coloradoense* and *Vascoceras* (*Paravascoceras*) cf. *cauvini* indicated the close proximity of the Cenomanian–Turonian boundary (Cooper, 1972, 1976, 1978). A Late Turonian–Early Coniacian age was assigned to sediments below the basalt and was based on the occurrence of *Vascoceras* cf. *proprium*, *Morrowites mocamedensis*, *Anagaudryceras involvulum*, *Hypophylloceras* sp., *Placenticeras kaffrarium*, *Tetragonites glabrus*, *Mossamedites serratarinatus*, *Puebloites greenhornensis*, *Prionocycloceras carvalhoi*, *Forresteria* sp., *Veniella forbesiana*, *Kossmaticeras theobaldianum*, *Mesopuzosia indopacifica* (Cooper, 2003a). Marine strata above the basalt produced the ammonites *Baculites* aff. *bailyi*, *Damesites sugata*, *Menuites* sp., *Hauericeras* (*Gardeniceras*) *gardeni*, *?Protexanites*, *Texanites venustus* and were considered Middle Santonian–Early Campanian in age (Cooper, 2003b). Marine amniote fossils and shark teeth recovered in the uppermost marine strata have been assigned a Late Campanian to Maastrichtian age (Antunes, 1964; Antunes and Cappetta, 2002; Cooper, 2003b; Bardet et al., 2005; Schulp et al., 2008, 2013; Polcyn et al., 2010; Bardet, 2012; Mateus et al., 2012). These age estimates constrain the chemostratigraphic age of marine strata at Bentiaba. Thus, carbon isotope data from Bentiaba appear to span nearly the entire Late Cretaceous and provide $\delta^{13}\text{C}$ data for

a time interval not well represented in the Southern Hemisphere or anywhere in the African continent.

2. Material and methods

2.1. Stratigraphy and sampling

Stratigraphic sections were measured by L.L. Jacobs, K. Ferguson, M.J. Polcyn, and C. Strganac in 2006, 2007, 2008, and 2010 (Fig. 2), and follow the general stratigraphy and nomenclature established in Cooper (1976, 2003a). Basalt samples and marine bivalve shells were collected where possible throughout the section. Basalt samples were examined in thin section and sent to the Department of Geological Sciences at Michigan State University for XRF analysis to examine the potential for providing a reliable radiometric age date. The best candidate, sample PA 322, was sent for $^{40}\text{Ar}/^{39}\text{Ar}$ radiometric age determination at the Arizona Noble Gas Laboratory. The details of the methodology used for $^{40}\text{Ar}/^{39}\text{Ar}$ radiometric age dating are provided in Appendix A.

2.2. Stable isotope analyses

Samples from fifty-five shells from 40 stratigraphic horizons were drilled near the hinges where the shell is thickest. Inoceramus samples were examined visually with scanning electron microscopy and chemically with energy-dispersive X-ray spectroscopy, revealing that some samples near the top of the section were dolomitized (Appendix B). Altered samples were rejected.

Samples were vacuum-sealed in reaction vessels with ortho-phosphoric acid, and left to react in a 25 °C bath for at least 4 h. The carbon dioxide gas produced from the reaction was cryogenically purified, then analyzed in a Finnigan MAT 252 mass spectrometer. The marine $\delta^{13}\text{C}$ isotopic curve derived from calcite in the shells from Bentiaba is compared to the English Chalk $\delta^{13}\text{C}$ stratigraphy (Jarvis et al., 2006; Voigt et al., 2010), Italy (Jenkyns et al., 1994; Voigt et al., 2012), South Atlantic core DSDP Site 525A (Li and Keller, 1999), and Southern Ocean core ODP Site 690C (Friedrich et al., 2009) to discern similarities in patterns.

2.3. Paleomagnetic and magnetostratigraphic analyses

Oriented samples were obtained by J. Salminen in 2012, along the measured section from the 50 m level to 135 m with 15–115 cm spacing where possible. One to three samples were taken from each sampling level and most samples were collected using a hand-held gasoline-powered drill with a 2.5 cm diameter bit. A few block samples were obtained from fragile sandstone. Samples were oriented using a magnetic compass combined with a sun compass.

Paleomagnetic measurements were carried out at the Solid Earth Geophysics Laboratory of the University of Helsinki, Finland. Stepwise alternating field (AF) demagnetizations were performed in 16 increasing steps with maximum field up to 160 mT using three-axis demagnetizer coupled with 2G-DC SQUID magnetometer. Thermal demagnetization procedures were carried out on sister specimens. AF demagnetization gave stable results, but thermal treatment failed for most of the specimens. Vector

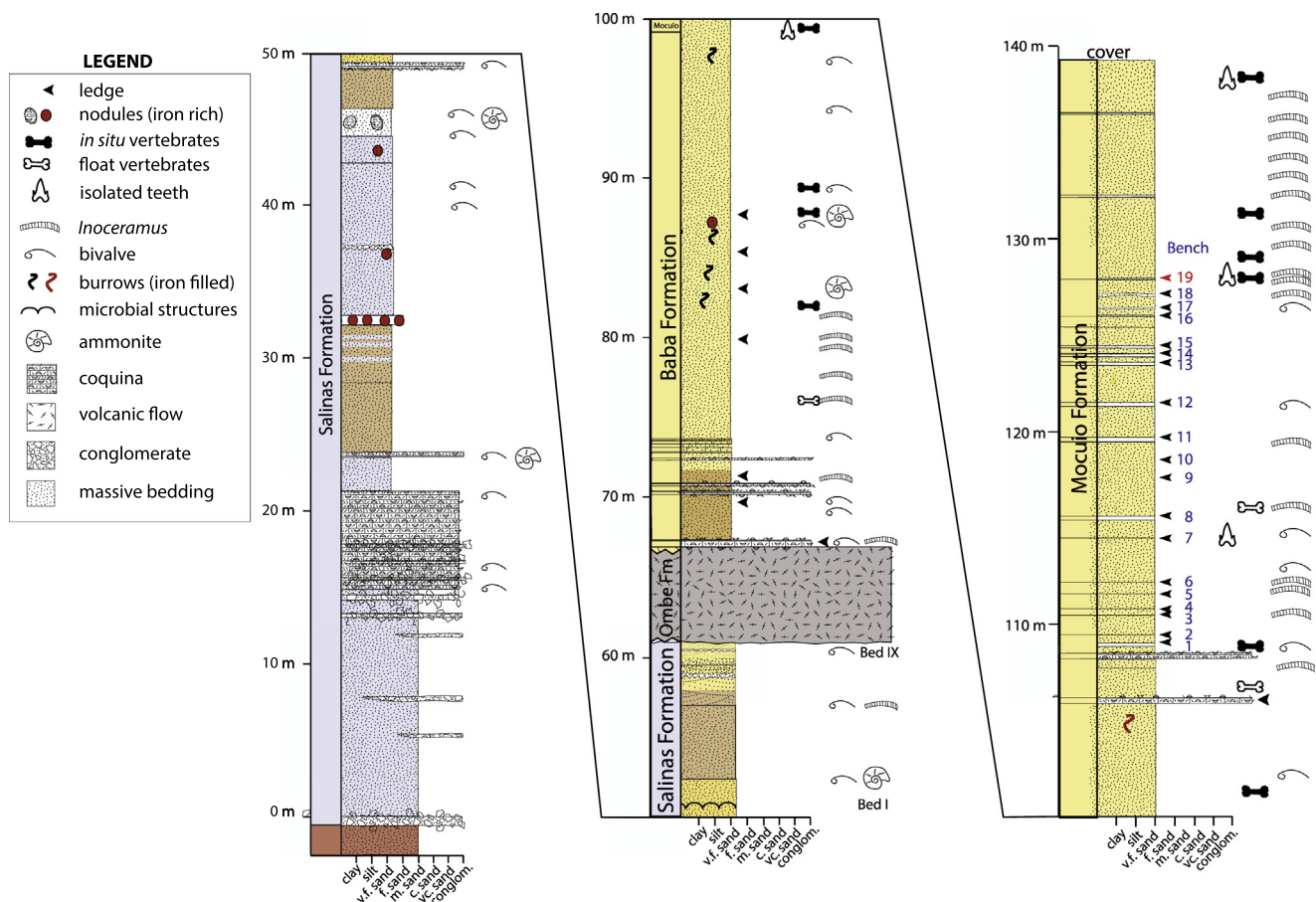


Fig. 2. Stratigraphic section at Bentiaba. Number 19 indicates stratigraphic horizon producing mosasaur fossils described in Jacobs et al. (2006), Schulp et al. (2008), Polcyn et al. (2010), and Mateus et al. (2012).

components were isolated using principal component analysis (Kirschvink, 1980). Components with Mean Angular Deviation (MAD) values less than 15° and in some cases less than 20° were accepted.

Husson et al. (2011) recently provided an astronomical calibration of the Maastrichtian geomagnetic polarity timescale, offering two age options for each polarity transition because of uncertainties with respect to long-term variation of the 405 Ka eccentricity cycle. This refined calibration modifies somewhat the timescale of Ogg and Hinnov (2012). For correlation we use Husson et al. (2011).

3. Results

3.1. Late Cretaceous stratigraphy at Bentiaba

The section measures strata that are gently folded with the axes trending northeast–southwest. The base of the section is the contact between the syn-rift Piambo Formation, composed of red sandstones and conglomerates about 20 m in exposed thickness. The shallow-water marine Salinas Formation unconformably overlies the Piambo Formation and is 60 m thick. The lowest 24 m of the Salinas are crossbedded blue–gray sands with intercalated cobble conglomerate channels, up to 30 cm thick, and two coquina layers. The stratigraphically higher coquina bed is 50 cm thick and underlies the lowest occurrence of tan-yellow fine sandstones and siltstones in the section.

Siltstone layers in the overlying 20 m alternate between blue–gray and tan and are predominantly massive. Calcified burrows and iron concretions are present in three beds. The top 10 m of the unit, Beds I through IX *sensu* Cooper (2003a), contain microbial structures and a Late Turonian–Early Coniacian ammonite fauna (Cooper, 2003a).

The Ombe Volcanic Formation is a 6 m thick basalt flow overlying the Salinas Formation. Pillow-shaped masses and hyaloclastites are present in the western portion of the exposure along the present shore, but one kilometer east the underlying shallow marine sediments are more deeply weathered and baked, indicating the basalt represents a flow at the Cretaceous coastline.

The contact with the overlying Baba Formation is disconformable. Rip-up clasts up to cobble size are present in the lowest 50 cm of the unit. The Baba Formation is about 45 m thick, and consists of alternating massive friable fine-grained sandstones, up to 10 m thick, and limestone cemented sandstone layers, 5–10 cm in thickness. Burrows are present in five of the thicker massive beds and the stratigraphically highest burrows are iron-filled. Shells belonging to marine bivalves, including inoceramids, are present throughout the Baba Formation, but most commonly occur in limestone-cemented layers. The lowest 10 m of the Baba Formation yielded ammonites Cooper (2003b) assigned to a Middle Santonian to Early Campanian age.

The contact of the Baba Formation with the overlying Mocuio Formation is irregular, with up to 5 cm of relief, and is marked by a 5 cm thick coquina. The Mocuio is similar to the Baba, containing alternating massive friable sandstones and more resistant carbonate-cemented sandstones that form the tops of benches. The lowest 20 m of the Mocuio Formation differs from the Baba Formation in having thinner massive beds, up to 2 m in thickness. At the nineteenth bench, abundant and diverse marine vertebrate fossils were collected (Schulp et al., 2008; Polcyn et al., 2010, 2013; Mateus et al., 2012). The uppermost Mocuio Formation consists of 10 m of massive friable sandstones that crop out about 100 m east of the coast. This part of the section also contains vertebrate fossils, including two new records of mosasaurs (Mateus et al., 2012; Schulp et al., 2013), but was not suitable for carbon

analysis or magnetostratigraphic sampling. Marine sediments, similar in lithology and stratigraphic position to the Mocuio Formation, crop out near Piambo and on top of the pre-Mesozoic basement.

3.2. Age of the Ombe Formation

The Ombe Formation is a transitional basalt based on the relative weight percentages of SiO_2 , K_2O , and Na_2O , and contains olivine phenocrysts in a groundmass primarily of plagioclase. Two splits of a single basalt sample BEN-002 were analyzed for age determination. The plateaus of the splits, shown in Fig. 3, were defined by 90% of the cumulative ^{39}Ar released and by 10–13 contiguous steps. The plateaus yielded ages within the Santonian, 83.7 ± 1.0 Ma and $85.5 \text{ Ma} \pm 0.8$ Ma. The average of the two splits, 84.6 Ma, is accepted as the age, and the standard deviation of ± 1.5 Ma was calculated from the two splits.

3.3. Paleomagnetism and magnetostratigraphy

We follow the convention for the Southern Hemisphere by referring to upward north-seeking directions as “normal” polarity and downward south-seeking directions as “reversed” polarity. Typical orthogonal projections of AF demagnetization are depicted in Zijderveldt diagrams in Fig. 4. Diagrams decay to origin indicating that characteristic high coercivity magnetization directions are adequately defined during AF demagnetization. In addition few successful thermal cleanings with unblocking temperature of $540\text{--}550^\circ\text{C}$ indicate that magnetite is the carrier of the primary remanent component. Both normal and reverse magnetization components were obtained. Magnetostratigraphic data are useful in the lower and upper portions of the section above the Ombe basalt, but these two segments are separated by nearly 30 m of section from which magnetic data was not recovered (Fig. 5).

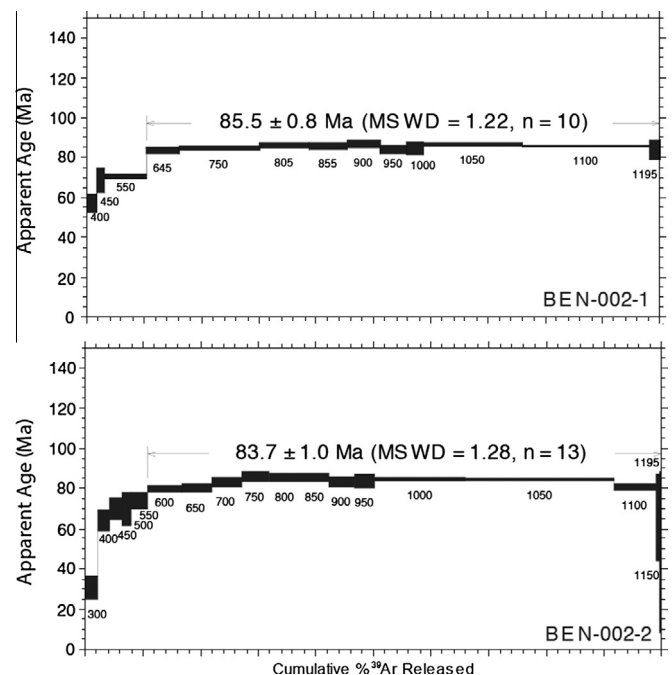


Fig. 3. Cumulative ^{39}Ar released in whole rock $^{40}\text{Ar}/^{39}\text{Ar}$ analysis of Ombe Formation basalt performed at Arizona Noble Gas Laboratory.

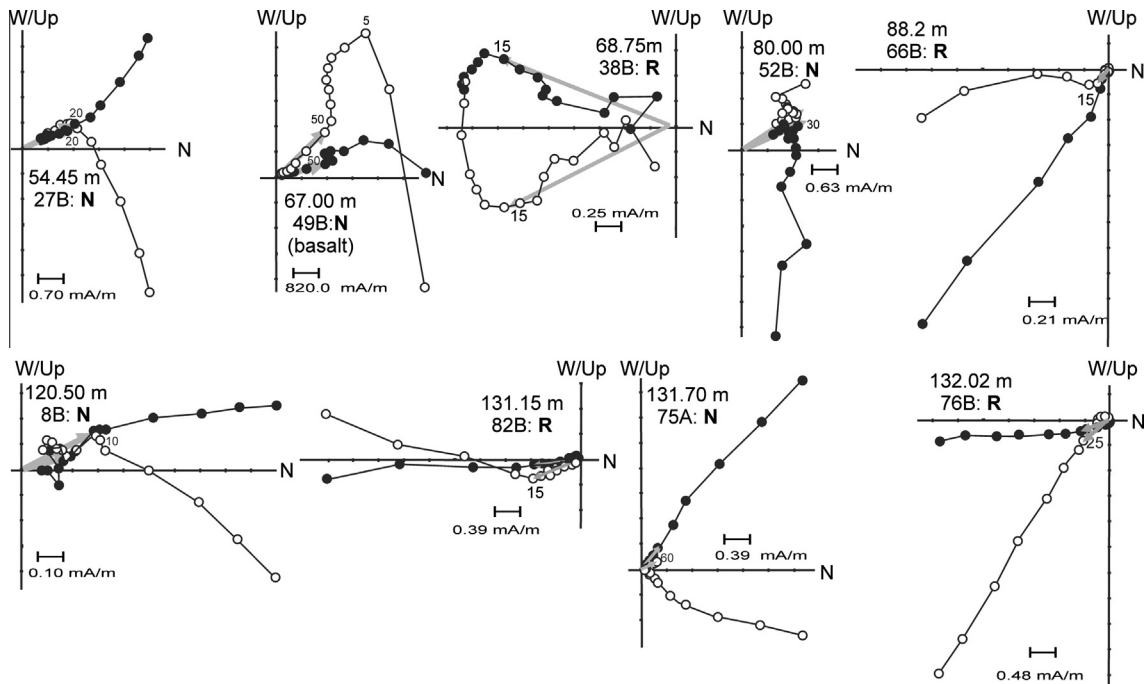


Fig. 4. Orthogonal projections of alternating field (AF) demagnetization data of Bentiaba samples. Closed (open) symbols represent projections on the horizontal (vertical) planes. Labels indicate meter levels for samples. N (R) indicate normal (reversed) polarity. Number at diagrams indicate af step in mT.

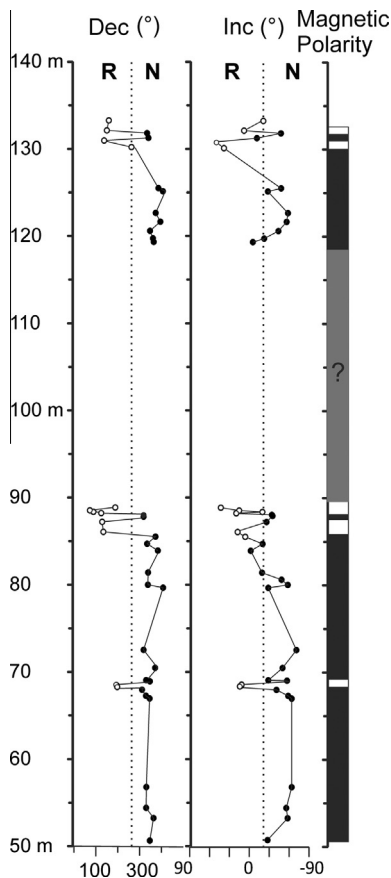


Fig. 5. The magnetostratigraphy of the Bentiaba section. Declination and inclination values of magnetization components are interpreted in terms of normal (black blocks) and reverse (white blocks) polarity zones. Gray in polarity chron column and the question mark indicates unsolved polarity. Each sampling level contains multiple samples.

3.4. Stable carbon isotopes

$\delta^{13}\text{C}$ values of shell and matrix samples are presented in Table 1 and comparisons of $\delta^{13}\text{C}$ to $\delta^{18}\text{O}$ are presented in Fig. 6. The coefficients of determination between $\delta^{13}\text{C}$ to $\delta^{18}\text{O}$ are low for all calcite samples, and for matrix ($R^2 = 0.03$), non-inoceramid bivalves ($R^2 = 0.11$) and inoceramids ($R^2 = 0.27$). There is a substantially higher correlation between $\delta^{13}\text{C}$ to $\delta^{18}\text{O}$ in dolomitized inoceramids ($R^2 = 0.56$), and the values are typically enriched in ^{13}C and are not used for the chemostratigraphy.

The stable carbon isotopic values for shells and rock are plotted against stratigraphic position and magnetostratigraphy in Fig. 7. The overall pattern shows a general trend of decreasing $\delta^{13}\text{C}$ value with stratigraphic height from 20 m to the basalt, and again in strata overlying the basalt. The $\delta^{13}\text{C}$ values in shells are generally more positive than those values yielded from matrix and are offset by $\sim 1\text{‰}$ in the pattern above the basalt.

The curve produced by shells, shown as the line in Fig. 7, indicates four major excursions of at least 1.5‰ deviating from the background $\delta^{13}\text{C}$ shell values of $\sim 1\text{‰}$ – 2‰ . Non-inoceramid bivalves recovered from the lower Salinas Formation show a positive $\sim 3\text{‰}$ excursion, obtained from sequential $\delta^{13}\text{C}$ values of 0.8‰ , 3.6‰ , and 0.9‰ derived from samples collected in triplicate and averaged at each level (15, 21, and 23 m from the base of the section). At 40 m, a negative excursion of $\sim 3\text{‰}$ is produced by bivalve shell values of 2.1‰ to -0.6‰ . A $\sim 1.5\text{‰}$ positive shift is produced by $\delta^{13}\text{C}$ values of 1.9‰ , 3.4‰ , and 2.0‰ in shells collected within the lowest 4 m of the Baba. At 105–115 m, there is a wide range in values from -2.1‰ to 2.3‰ . Averaging these sample values across this interval results in a negative $\sim 3\text{‰}$ shift resulting from 1.0‰ , -2.1‰ , and 1.3‰ .

4. Discussion

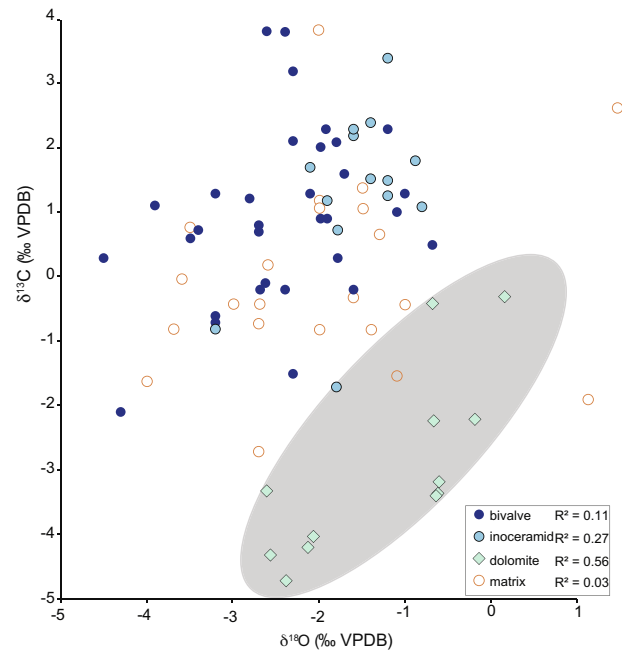
The Bentiaba $\delta^{13}\text{C}$ chemo- and magnetostratigraphy (Fig. 7) are anchored by the 84.6 ± 1.5 Ma Ombe basalt and is presented in Fig. 8. The age of the basalt and its normal polarity, taken with

Table 1
Stable isotope values for shells and matrix. Asterisk indicates dolomitized carbonate.

Height (m)	Sample #	Taxon	$\delta^{13}\text{C}$	$\delta^{18}\text{O}$
139.5	PA 457	Inoceramid*	-3.4	-0.6
138.5	PA 456	Inoceramid*	-4.2	-2.1
137.5	PA 456	Inoceramid*	-3.4	-0.6
136.5	PA 455	Inoceramid*	-4.3	-2.5
135.5	PA 454	Inoceramid*	-3.2	-0.6
134.5	PA 452	Inoceramid*	-4.7	-2.4
134.5	PA 451	Inoceramid*	-2.2	-0.2
134.5	PA 373	Inoceramid*	-4.0	-2.0
131.5	PA 372	Inoceramid*	-3.3	-2.6
129	PA 371	Inoceramid*	-2.2	-0.6
128	PA 372	Bulk	-2.0	1.1
128	PA 386	Inoceramid	0.7	-1.8
127	PA 370	Bulk	-0.8	-1.4
127	PA 370	Inoceramid	1.5	-1.2
124	PA 384	Bivalve	-0.2	-1.6
119	PA 383	Inoceramid	1.3	-1.2
116	PA 382	Bulk	-1.5	-1.1
116	PA 382	Inoceramid	-1.7	-1.8
115.5	PA 369	Inoceramid*	-0.3	0.2
115	PA 381	Inoceramid*	-0.4	-0.7
113	PA 380	Bivalve	-1.5	-2.3
112.5	PA 379	Bivalve	-2.1	-4.3
112	PA 389B	Bivalve	0.5	-0.7
112	PA 389B	Bulk	-0.3	-1.6
111	PA 389A	Bivalve	-0.2	-2.4
110.5	PA 367	Bulk	-0.4	-1.0
110.5	PA 367	Inoceramid	1.1	-0.8
108	PA 409	Bivalve	0.3	-1.8
108	PA 368	Inoceramid	1.8	-0.9
106	PA 365	Bivalve	1.0	-1.1
106	PA 408	Bivalve	2.3	-1.2
106	PA 407	Bivalve	1.3	-1.0
106	PA 407	Bulk	-0.8	-2.0
97	PA 375	Bivalve	0.9	-1.9
94	PA 376	Bivalve	1.6	-1.7
94	PA 376	Bulk	1.1	-1.5
89	PA 377	Bivalve	1.3	-2.1
87	PA 378	Bivalve	0.9	-2.0
87	PA 378	Bulk	0.7	-1.3
81	PA 364	Inoceramid	1.5	-1.4
80	PA 363	Inoceramid	2.2	-1.6
79	PA 362	Inoceramid	2.4	-1.4
77	PA 361	Bulk	1.2	-2.0
77	PA 361	Inoceramid	1.2	-1.9
73	PA 359	Bivalve	2.0	-2.0
73	PA 359	Bulk	0.0	-3.6
71	PA 358	Bulk	1.1	-2.0
71	PA 358	Inoceramid	2.3	-1.6
69.5	PA 357	Inoceramid	3.4	-1.2
69	PA 356	Bivalve	2.3	-1.9
69	PA 356	Bulk	1.4	-1.5
67	PA 355	Bivalve	2.1	-1.8
67	PA 355	Bulk	2.4	1.3
67	PA 355	Inoceramid	1.7	-2.1
60	PA 525	Bivalve	-0.2	-2.7
60	PA 525	Bulk	-0.4	-2.7
57	PA 392	Bulk	-0.7	-2.7
57	PA 392	Inoceramid	-0.8	-3.2
50	PA 443	Bulk	-0.8	-3.7
49	PA 393	Bivalve	-0.7	-3.2
49	PA 442	Bulk	0.2	-2.6
49	PA 393	Bulk	-1.6	-4.0
48	PA 440	Bivalve	-0.1	-2.6
45	PA 439	Bivalve	-0.6	-3.2
42	PA 438	Bivalve	1.3	-3.2
41	PA 437	Bivalve	2.1	-2.3
23	PA 394	Bivalve	0.8	-2.7
23	PA 394	Bivalve	0.7	-2.7
23	PA 394	Bivalve	1.2	-2.8
23	PA 394	Bulk	-2.7	-2.7
21	PA 395	Bivalve	3.2	-2.3
21	PA 395	Bivalve	3.8	-2.4
21	PA 395	Bulk	3.9	-2.0
15	PA 396	Bivalve	1.1	-3.9

Table 1 (continued)

Height (m)	Sample #	Taxon	$\delta^{13}\text{C}$	$\delta^{18}\text{O}$
15	PA 396	Bivalve	0.7	-3.4
15	PA 396	Bivalve	0.6	-3.5
15	PA 396	Bulk	0.8	-3.5
14	PA 398	Bivalve	0.3	-4.5

**Fig. 6.** $\delta^{13}\text{C}$ plotted against $\delta^{18}\text{O}$ for inoceramids, other bivalves, and matrix samples from Bentiaba.

the normal polarity and Turonian ammonite fauna of the upper Salinas Formation below the basalt is consistent with placement of these strata in chron C34n, also known as the Cretaceous Normal-Polarity Super Chron or the “Cretaceous Quiet Zone.” The large $\sim 3\text{‰}$ carbon excursion in the Salinas Formation correlates to the Cenomanian–Turonian Boundary Event, which is observed regionally as a $\sim 4\text{‰}$ positive excursion in bulk organic carbon isotopes at Walvis Ridge DSDP Site 530A (Forster et al., 2008), and globally as a $>2.0\text{‰}$ positive excursion in marine and terrestrial records at OAE 2 (Gale et al., 2005; Jarvis et al., 2006; Hasegawa et al., 2013). The correlation is supported by a Late Cenomanian ammonite fauna from the base of the Salinas Formation and float specimens of the Early Turonian ammonites *Watinoceras coloradoense* and *Vasoceras (Paravasoceras) cf. cauvini* (Cooper, 1972, 1976, 1978). No magnetostratigraphic samples were analyzed at this level because of the pre-Santonian age determined by the age of the overlying Ombe basalt, and therefore we assume the strata of the Bentiaba section below those sampled for magnetostratigraphy would fall in the Cretaceous Quiet Zone.

The negative $\sim 3\text{‰}$ excursion high in the Salinas Formation with normal magnetization, is correlated to minimum $\delta^{13}\text{C}$ values observed during the Late Turonian in sections of the English Chalk (Jarvis et al., 2006). There is a broad positive excursion in the English Chalk and Gubbio reference curves during the Coniacian (Jenkyns et al., 1994; Jarvis et al., 2006) that is absent in our data and suggests the Coniacian is missing from Bentiaba. A Late Turonian age is consistent with the Late Turonian–Early Coniacian biostratigraphic assignment of ammonite faunas from the upper Salinas

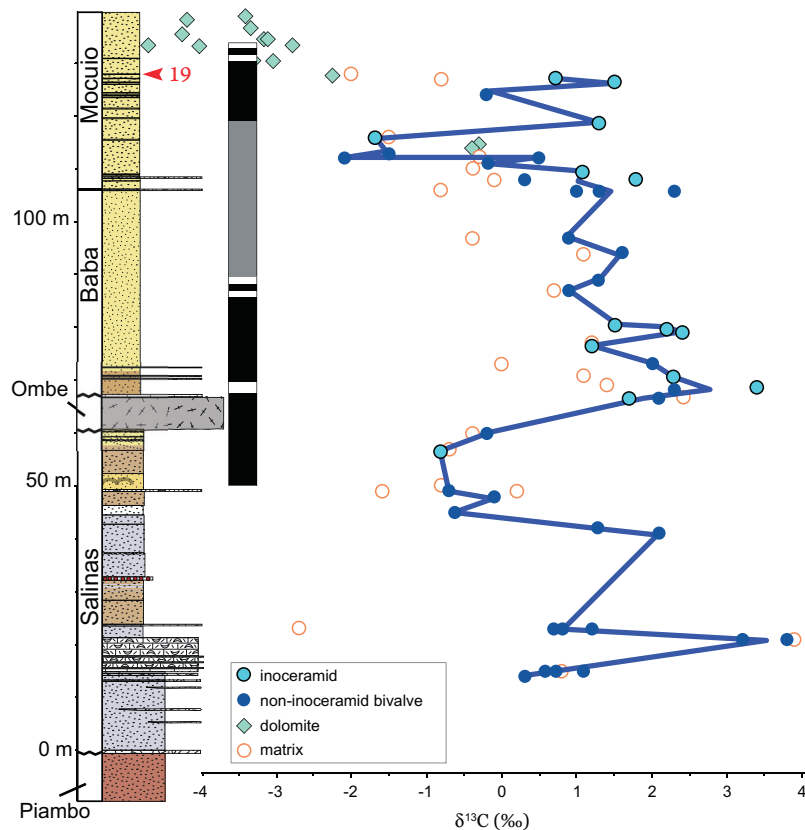


Fig. 7. $\delta^{13}\text{C}$ values for shells and matrix plotted against stratigraphic and magnetostratigraphic position. Line represents curve for shell values and crosses average value at stratigraphic heights where multiple shells were sampled.

Formation (Cooper, 1972, 1976, 2003a). The Coniacian age described by Cooper (2003a) was based on a partial ammonite belonging to the genus *Forresteria*, which is also known from the Late Turonian (Cobban et al., 2006). The age of the Bentiaba basalt falls within the Santonian stage, generally consistent with the ammonite biostratigraphy presented by Cooper (1972, 1976, 1978, 2003a,b).

We correlate the lowest reversed signal, directly above the Ombe basalt, with chron C33r, which constrains the youngest age for the Ombe basalt at the C34n/C33r boundary at 83.6 Ma. The normal interval from 68 to 85 m in section is C33n, followed by a reversed couplet representing the base of C32, that is, C32r.2r, C32r.1n, and C32r.1r, with age limits of 74.1–73.6 Ma (Husson et al., 2011). The 30 m above the reversed couplet has no recoverable paleomagnetic data; however, by integrating the pattern in $\delta^{13}\text{C}$ chemostratigraphy and vertebrate biostratigraphy, we interpret the normal recovered between 119 m to 126 m to represent C32n.1n (see discussion below). Therefore C32n.2n and C32n.1r are subsumed in the interval with no recoverable data. The paleomagnetic reverse-normal couplet are C31 and the reverse polarity at 132.5 m indicates an age of 68.32 ± 0.07 Ma (Husson et al., 2011).

The $\sim 1.5\text{‰}$ excursion at the base of the Baba Formation falls in a reversed magnetozone recognized here as chron C33r and correlated to the Santonian–Campanian Boundary Event found low in C33r in the English Chalk, Tethys, and Western Interior Seaway (Jenkyns et al., 1994; Jarvis et al., 2006; Wagreich, 2012). While the composite English Chalk reference curve characterizes the Santonian–Campanian Boundary Event as a positive 0.3‰ excursion, the excursion in the Baba Formation is consistent with maximum excursion values of 2.9‰ reported by Jarvis et al. (2006). The Campanian age estimated for the Baba Formation agrees with the

youngest biostratigraphic age limit of Cooper (2003b). Moreover, the correlation of the carbon curve, if correct, constrains the reversed portion of the lower Baba to the base of C33r, demonstrating that most of its 4.2 my duration is missing.

The reversed couplet at Bentiaba above C33n is correlated to C32r.2r, C32r.1n, and C32r.1r, at the base of chron C32. In turn, the negative carbon excursion above C33r but below the reversed couplet may be correlated to the Late Campanian Event (~ 75.5 Ma) observed in shelf-sea sections (Jarvis et al., 2006; Voigt et al., 2010, 2012; Thibault et al., 2012a,b). The magnitude of the excursion at Bentiaba is greater than the $<0.3\text{‰}$ excursion observed in the English Chalk and Gubbio reference sections (Jarvis et al., 2006; Voigt et al., 2012), but it is correlated to the Late Campanian Event because this negative excursion represents the $\delta^{13}\text{C}$ minimum below the C32 reversed couplet (C32r.2r, C32r.1n, and C32r.1r). This correlation, if correct, implies that not only the middle and upper portions of C33r is missing, but the lower and middle portions of C33n as well, indicating that a substantial portion of the lower and middle Campanian is missing and that net sedimentation rates increased during the Late Campanian.

A negative 3‰ $\delta^{13}\text{C}$ excursion at the base of the Mocuio Formation is correlated with the Campanian–Maastrichtian Boundary Events in the Boreal Chalk Sea, Tethys, Atlantic, Indian, and Pacific Oceans (Li and Keller, 1999; Friedrich et al., 2009; Voigt et al., 2012; Thibault et al., 2012a,b). The excursion in the Mocuio Formation is substantially greater in magnitude than the negative $<1.0\text{‰}$ excursions spanning the Campanian–Maastrichtian Boundary in the reference sections, but these events in the reference sections are the largest negative excursions during the Late Cretaceous and fall within the normal polarity of C32n.2n.

The positive shift in $\delta^{13}\text{C}$ to values $\sim 1\text{‰}$ at 119 m are correlated to $\delta^{13}\text{C}$ maximum values in chron 32n.1n recovered in Gubbio and

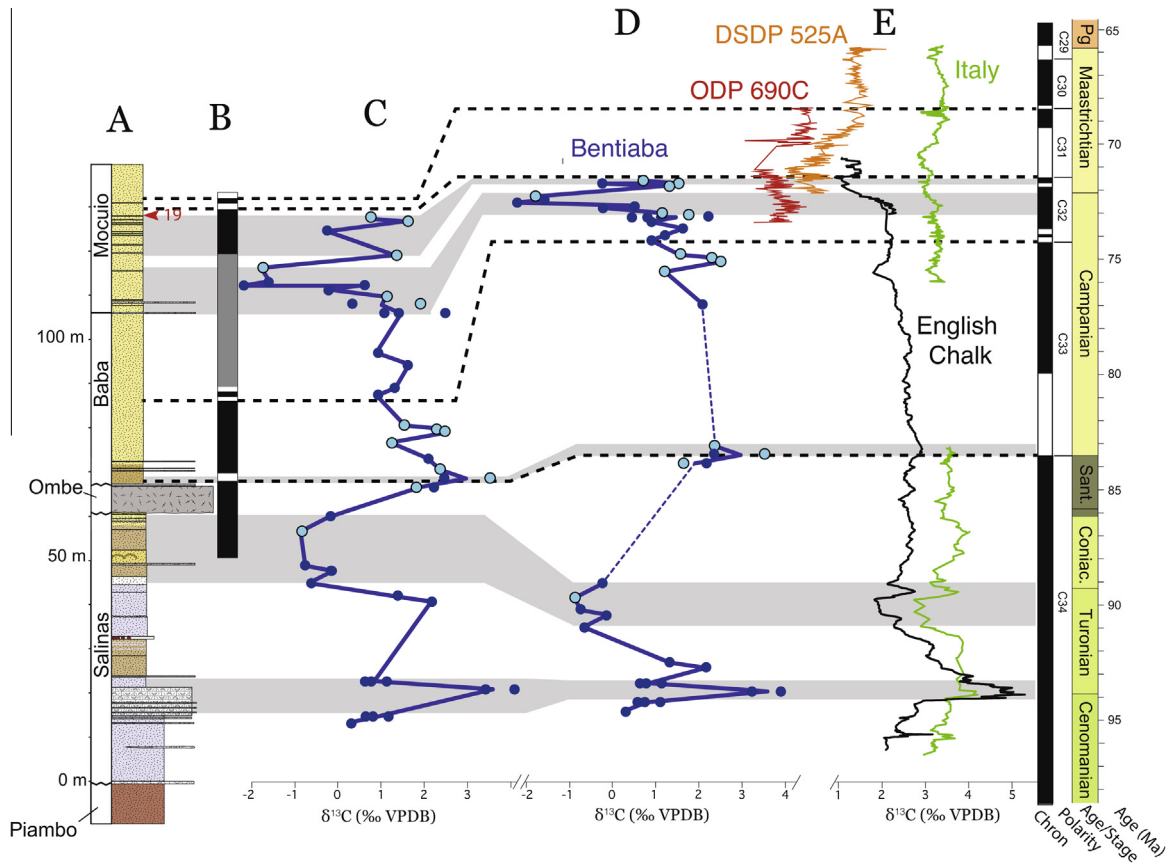


Fig. 8. $\delta^{13}\text{C}$ chemostratigraphy and magnetostratigraphy of Bentiaba section. (A) Generalized section at Bentiaba. Arrow points to bench 19 referred to in text. (B) Magnetostratigraphy for Bentiaba. (C) Bentiaba $\delta^{13}\text{C}$ values plotted in stratigraphic position. (D) Bentiaba $\delta^{13}\text{C}$ curve scaled vertically, and dashed to indicate significant gaps in record. (E) Reference $\delta^{13}\text{C}$ curves of the English Chalk (Jarvis et al., 2006; Voigt et al., 2010 in bold), Italy (Jenkyns et al., 1994; Voigt et al., 2012), South Atlantic core DSDP Site 525A (Li and Keller, 1999), and Southern Ocean core ODP Site 690C (Friedrich et al., 2009). Curves for Italy and ODP Site 690C are offset by $+1.0\text{‰}$ and -1.0‰ , respectively, for clarity. Curves of Jenkyns et al. (1994) and Jarvis et al. (2006) are adjusted to reflect the updated time scale of Ogg and Hinnov (2012). Global paleomagnetic log follows Ogg and Hinnov (2012) prior to the Late Campanian and Late Campanian–Maastrichtian of Husson et al. (2011) and dashed lines indicate the correlated chron boundaries. Shaded region on time scale shows age of the Ombe Formation basalt.

the Walvis Ridge (Tie-point 7 *sensu* Voigt et al., 2012; their Table 2). The implications of this correlation are that the entire C32n.2n and C32n.1r and potentially part of C32n.1n and C32r.1r fall in the 30 m of unrecoverable magnetic data in the upper Baba and Mocuio formations. Because C32n.1r spans ~ 80 kyr (Husson et al., 2011), the reversal, if it were present, would be represented by ~ 20 cm in the unrecovered interval.

Global correlations of the Baba and Mocuio formations at Bentiaba suggest that the initial deposition of the Baba Formation was the earliest Campanian, at C34/C33 at 84.6 Ma (Ogg and Hinnov, 2012) indicated by the Santonian–Campanian Event in the $\delta^{13}\text{C}$ curve, although the thinness of C33r relative to C33n indicates most of the lower Campanian is missing or condensed. The Mocuio Formation extends from the latest Campanian to Early Maastrichtian, with a limit of 68.32 Ma placed by C30n/C31r at 133 m in section.

The mosasaur fossil record supports the correlations we have proposed for the Mocuio Formation. The most productive level for vertebrate fossils at Bentiaba is Bench 19, which has yielded six taxa of mosasaurs (Jacobs et al., 2006; Schulp et al., 2008; Polcyn et al., 2010; Mateus et al., 2012). Of these, *Prognathodon kiana* is endemic to Angola so far as known (Schulp et al., 2006, 2008) and "*Platecarpus*" *ptychodon* is endemic to Africa, known from the Maastrichtian of Morocco, Nigeria, and Angola. *Halisaurus* sp., known from Bentiaba, appears to range from Lower to Upper Maastrichtian in Morocco (Bardet, 2012). *Mosasaurus hoffmani* appears worldwide in the Early Maastrichtian (Jagt, 2005;

Kiernan, 2002) and is present immediately above Bench 19. *Phosphorosaurus*, otherwise known only from the Early Maastrichtian of Europe (Jagt, 2005), is present as float above Bench 19. *Globidens phosphaticus* disappears globally with the large bivalve *Inoceramus* before the end of the Maastrichtian (Polcyn et al., 2010).

Most of the mosasaur taxa known from Bentiaba are also known from Morocco, where sediments are reported to range from Lower to Upper Maastrichtian based on biostratigraphy, especially of elasmobranchs (Capetta, 1987; Bardet et al., 2005; Bardet, 2012). More specifically, large *Prognathodon* and *Carinodens* (Schulp et al., 2013), which are also known from the top of the Bentiaba section above levels sampled for magnetostratigraphy, only occur in the Late Maastrichtian in Morocco (Bardet, 2012). Likewise, *Carinodens* in North America and Europe is only known from the Late Maastrichtian (Jagt, 2005; Mulder et al., 2013).

Younger strata at Bentiaba that could not be sampled for magnetostratigraphy occur above the magnetic and isotopic sections presented here and our fieldwork has produced numerous vertebrate fossils from them, specifically *Carinodens* and a large species of *Prognathodon* (Schulp et al., 2013). The large *Prognathodon* is at a morphological grade similar to that of *P. saturator* from the Late Maastrichtian of Europe, and is thus consistent with Late Maastrichtian faunas of Morocco and Europe (Mateus et al., 2012; Schulp et al., 2008, 2013). Moreover, no Paleogene fossils of any sort have been recovered from the Bentiaba section, and the section is truncated immediately above the occur-

rence of the large *Prognathodon*. Therefore, the presence of Late Maastrichtian mosasaurs high in the section weigh against a correlation of the top of the magnetostratigraphic section with C29r, which includes the K–Pg boundary. The $\delta^{13}\text{C}$ stratigraphy and magnetostratigraphy presented here places the mosasaur-bearing strata at Bench 19 in the Bentiaba section within the top of C32n.1n, at about 71.5 Ma.

Polcyn et al. (2013) discussed the evolution of mosasaurs as being driven by productive seas that provided unlimited food resources (bottom-up selection), driving size disparity and niche differentiation among top consumers. During the growth of the South Atlantic, mosasaurs and other top predators were abundant along coastal Angola, benefitting from upwelling-generated productivity as Africa drifted northward through subtropical latitudes (Jacobs et al., 2009, 2011). The initiation of the northward drift of Africa

that facilitated extended productivity was coincident with Ombe Formation volcanism at Bentiaba.

The age of the basalt at Bentiaba is older than those of the Kwanza basin (Marzoli et al., 1999), but the composition conforms to the trend of increased alkalinity from the flood volcanism of the Etendeka–Paraná LIP to alkali basalts found as flows and dikes along the Atlantic margins in Africa and South America from 90 to 60 Ma (Marzoli et al., 1999; Torsvik et al., 2009; Comin-Chiaromonti et al., 2011). The age of the Bentiaba basalt is synchronous with a decrease in the drift rate and change in pole of rotation of the African continent (Torsvik et al., 2009) and with widespread deformation across the African continent during the Santonian (Guiraud et al., 1992; Bosworth et al., 1999). The occurrence of the Ombe basalt not only corresponds in age with these tectonic events, but if the correlations presented here are correct, the basalt

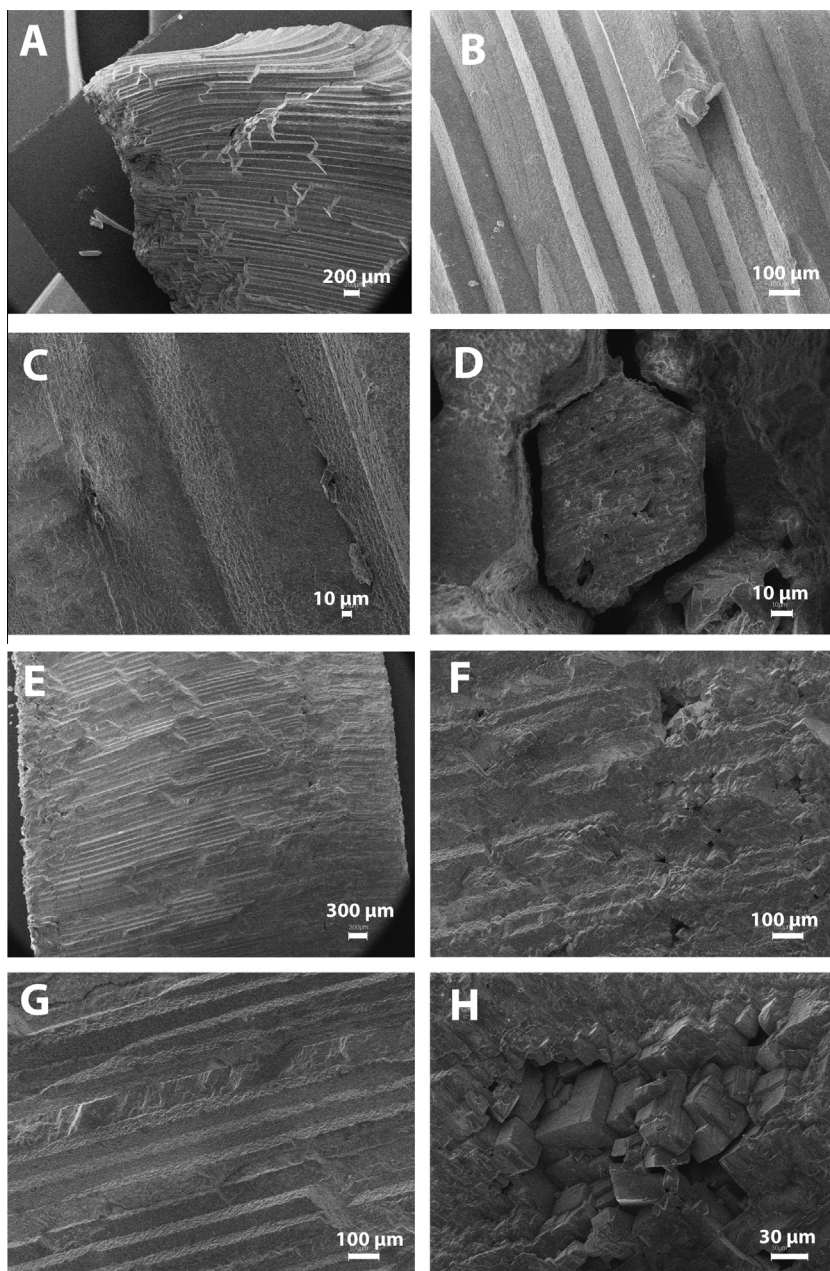


Fig. B1. SEM images of inoceramid prism structure of samples PA 357 (A–D) and PA 456 (E–H). A–C and E–H are views along the prism axis and D shows prism cross section.

Table B1
Atomic percent in shell samples estimated by electron dispersive spectroscopy.

Element								
Sample	C	O	Mg	Ca	Fe	Na	S	Al
PA 456	26.13	53.21	9.08	11.29	0.29	–	–	–
PA 456	24.83	54.08	9.46	11.36	0.28	–	–	–
PA 456	27.98	55.67	9.26	6.78	0.32	–	–	–
PA 364	23.45	55.72	0.38	20.46	–	–	–	–
PA 358	25.48	54.5	0.53	18.9	–	–	–	–
PA 451	26.02	55.3	8.86	8.75	0.28	–	–	–
PA 358	25.48	54.5	0.53	18.9	–	–	–	–
PA 357	23.64	53.59	0.35	20.87	–	0.49	0.62	–
PA 370	23.46	57.37	0.42	15.8	–	0.42	–	–
PA 370	20.28	56.14	1.95	19.22	0.57	–	–	1.84

and a thin veneer of sediment overlying it are the only remaining rock record of events of this interval known in the Namibe Basin.

5. Conclusions

The marine section at Bentiaba spans a 30 million year interval that encompasses most of the Late Cretaceous during the growth of the South Atlantic Ocean. Significant carbon isotope events, including Oceanic Anoxic Event 2 at the Cenomanian–Turonian Boundary, are identified in a $\delta^{13}\text{C}$ chemostratigraphic section for the ancient South Atlantic coast at Bentiaba calibrated by a radiometric age on a basalt and by magnetostratigraphy. The resulting correlations provide the African coast of the South Atlantic Ocean with a link, albeit discontinuous, to $\delta^{13}\text{C}$ patterns observed globally spanning almost the entire Late Cretaceous. Moreover, the results refine previous biostratigraphic age estimates for the sequence and allow biostratigraphic correlation to North Africa and other regions of the globe. The 84.6 Ma age of the Ombe basalt is synchronous with large-scale magmatic activity in the South Atlantic Ocean Basin and tectonism across much of the African continent and heralds the northward drift of Africa through productive upwelling latitudes, attesting to the physical drivers of marine top consumers such as mosasaurs, which dominated the seas for the last thirty million years of the Cretaceous.

Acknowledgments

This publication results from Projecto PaleoAngola, an international cooperative research effort among the contributing authors and their institutions, funded by the National Geographic Society, the Petroleum Research Fund of the American Chemical Society, Sonangol E.P., Esso Angola, Fundação Vida of Angola, LS Films, Maersk, Damco, Safmarine, ISEM at SMU, The Royal Dutch Embassy in Luanda, TAP Airlines, Royal Dutch Airlines, The Saurus Institute, and the Perot Museum of Nature and Science. JS was additionally funded by Yale University and the Alfred Kordelin Foundation. We dedicate this contribution to the late Kalunga Lima, our friend and colleague in Projecto PaleoAngola. We thank Margarida Ventura and André Buta Neto for providing our team help in the field. Tako and Henriette Koning provided valuable support and friendship in Angola. We thank Tyrone Rooney of Michigan State University for XRF examination on the Ombe basalt.

Appendix A. Arizona Noble Gas Laboratory $^{40}\text{Ar}/^{39}\text{Ar}$ radiometric dating methodology (Clark Isachsen, pers. comm.)

Whole rock chips for $^{40}\text{Ar}/^{39}\text{Ar}$ analysis were irradiated at the USGS TRIGA Reactor, Denver, Colorado along with GA1550 biotite 98.79 ± 0.54 Ma (Renne et al., 1998) flux monitors to calculate J-factors and K_2SO_4 and CaF_2 salts for interfering neutron reactions.

Following a 2–3 week cooling period to allow for the decay of short-lived isotopes, samples were loaded into the arms of a glass storage tree above a double-vacuum, resistance-heated furnace and heated to 120° at the same time that the entire extraction line was baked for 48 h at 220°C . Getters and furnace were independently degassed near the end of the bake-out. Samples were then dropped into the furnace and argon was extracted from each sample using a computer controlled step-heating routine. The temperature of the furnace is estimated to be accurate to $\pm 20^\circ\text{C}$. Each heating step had a duration of 12 min followed by a cool down to 500°C prior to advancing the gas into two successive gettering stages for argon purification. The argon was then admitted into a VG 5400 mass spectrometer, where it was ionized and detected by a VG electron multiplier and digitized with a Keithley 617 Electrometer. Data collection and processing were accomplished using the computer program Mass Spec (Deino, 2001). The decay constants used were those recommended by Steiger and Jäger (1977). Baseline values were subtracted and the isotopic measurements then were regressed to time zero using standard linear regression techniques. Additional corrections and associated uncertainties were applied to account for blanks, machine discrimination, atmospheric contribution, and interfering isotopes produced in the reactor from Ca, K and Cl present in the samples.

Appendix B. Dolomitization of rejected samples

Scanning electron analysis of inoceramids recovered from 57 to 110 m and 118 to 128 m in the section show intact prism structure with no visible crystal overgrowth, shown in Fig. B1 A–D. Additionally prism boundaries are clearly defined when looking down the axis of prism growth, shown in Fig. B1 D. Inoceramids recovered at 116 m in the section and above 128 m in the section, Fig. B1 E–H, show euhedral crystal growth in voids and on prisms. This crystal growth is restricted to 5 mm on the outside and inside margins of the shell but is not consistent in placement.

Electron dispersive analyses performed showed shells have a near uniform composition, and these are summarized in Table B1. Those with no visible alteration are ~55% oxygen, 24% carbon, 20% calcium, and <1.0% magnesium. Inoceramids with visible alteration are ~54% oxygen, 25% carbon, 11% calcium, 9% magnesium, and <1.0% iron. X-ray diffraction analyses also resulted in compositional differences between shells with and without crystal growth. Non-inoceramid bivalves and relatively intact inoceramids have primary 2-theta peaks at 30.0° , 47.5° , and 48.6° , corresponding with calcite. Inoceramids with visible crystal overgrowth are composed of dolomite indicated by primary peaks of 30.8° , 50.2° , and 50.8° .

References

- Antunes, M.T., 1964. O neocretácico e o cenozóico do litoral de Angola. Junta de Investigações do Ultramar, Lisboa, 254 pp.
- Antunes, M.T., Cappetta, H., 2002. Sélaciens du Crétacé (Albien–Maastrichtien) d'Angola. *Palaeontographica* 12, 85–146.
- Arthur, M.A., Dean, W.E., Pratt, L.M., 1988. Geochemical and climatic effects of increased marine organic carbon burial at the Cenomanian/Turonian boundary. *Nature* 35, 714–717.
- Bardet, N., 2012. Maastrichtian marine reptiles of the Mediterranean Tethys: a paleobiological approach. *Bull. Soc. Géol. France* 183 (6), 573–596.
- Bardet, N., Superbiola, X.P., Iarochene, M., Bouya, B., Amaghaz, M., 2005. A new species of *Halisaurus* from the Late Cretaceous phosphates of Morocco, and the phylogenetical relationships of the Halisaurinae (Squamata: Mosasauridae). *Zool. J. Linnean Soc.* 143, 447–472.
- Bosworth, W., Guiraud, R., Kessler II, L.G., 1999. Late Cretaceous (ca. 84 Ma) compressive deformation of the stable platform of northeast Africa (Egypt): far-field stress effects of the “Santonian event” and origin of the Syrian arc deformation belt. *Geology* 27 (7), 633–636.

- Burke, K., Gunnell, Y., 2008. The African erosion surface: a continent-scale synthesis of geomorphology, tectonics, and environmental change over the past 180 million years. *Geol. Soc. Am., Memoir* 201, 66 pp.
- Capetta, H., 1987. Mesozoic and Cenozoic Elasmobranchii, *Chondrichthyes* II. In: Schultze, H.P. (Ed.), *Handbook of Paleichthyology*, vol. 3B. Gustav Fischer Verlag, Stuttgart, New York.
- Carvalho, G.S. de., 1961. Geologia do deserto de Moçâmedes (Angola). *Memórias da Junta de Investigações do Ultramar* 26, 227 pp.
- Cobban, W.A., Walaszczyk, I., Obradovich, J.D., McKinney, K.C., 2006. A USGS Zonal Table for the Upper Cretaceous Middle Cenomanian–Maastrichtian of the Western Interior of the United States based on Ammonites, Inoceramids, and Radiometric Ages. U.S. Geological Survey, Open-File, Report 2006-1250, 46 pp.
- Comin-Chiaromonte, P., De Min, A., Girardi, V.A.V., Ruberti, E., 2011. Post-Paleozoic magmatism in Angola and Namibia: a review. In: Beccaluva, L., Bianchini, G., Wilson, M. (Eds.), *Volcanism and Evolution of the African Lithosphere*. Geological Society of America, Special Paper 478, pp. 223–247.
- Cooper, M.R., 1972. The Cretaceous stratigraphy of San Nicolau and Salinas, Angola. *Ann. S. Afr. Museum* 60 (8), 245–251.
- Cooper, M.R., 1976. The Mid-Cretaceous (Albian/Turonien) Biostratigraphy of Angola. *Annales du Muséum d'Histoire Naturelle de Nice* 4, XVI.1–XVI.22.
- Cooper, M.R., 1978. Uppermost Cenomanian-basal Turonian ammonites from Salinas, Angola. *Ann. S. Afr. Museum* 75 (5), 51–152.
- Cooper, M.R., 2003a. Upper Cretaceous (Turonian–Coniacian) ammonites from São Nicolau, Angola. *Ann. S. Afr. Museum* 110 (2), 89–146.
- Cooper, M.R., 2003b. Stratigraphy and paleontology of the Upper Cretaceous (Santonian) Baba Formation at São Nicolau, Angola. *Ann. S. Afr. Museum* 110 (3), 147–170.
- Deino, A.L., 2001. *Users Manual for Mass Spec v. 5.02*. Berkeley Geochronology Center Special, Publication 1a.
- Forster, A., Kuypers, M.M.M., Turgeon, S.C., Brumsack, H.-J., Petrizzo, M.R., Sinninghe Damsté, J.S., 2008. The Cenomanian/Turonian Oceanic Anoxic Event in the South Atlantic: new insights from a geochemical study of DSDP Site 530A. *Palaeogeogr. Palaeoclimatol. Palaeoecol.* 267, 256–283.
- Friedrich, O., Herrle, J.O., Wilson, P.A., Cooper, M.J., Erbacher, J., Hemleben, C., 2009. Early Maastrichtian carbon cycle perturbation and cooling event: implications from the South Atlantic Ocean. *Paleoceanography* 24, PA2211.
- Gale, A.S., Kennedy, W.J., Voigt, S., Walaszczyk, I., 2005. Stratigraphy of the Upper Cenomanian–Lower Turonian chalk succession at Eastbourne, Sussex, UK: ammonites, inoceramid bivalves and stable carbon isotopes. *Cretac. Res.* 26, 460–487.
- Guiraud, R., Binks, R.M., Fairhead, J.D., Wilson, M., 1992. Chronology and geodynamic setting of Cretaceous–Cenozoic rifting in West and Central Africa. *Tectonophysics* 213, 227–234.
- Hasegawa, T., Crampton, J.S., Schiøler, P., Field, B., Fukushi, K., Kakizaki, Y., 2013. Carbon isotope stratigraphy and depositional oxia through Cenomanian/Turonian boundary sequences (Upper Cretaceous) in New Zealand. *Cretac. Res.* 40, 61–80.
- Husson, D., Galbrun, B., Laskar, J., Hinnov, L.A., Thibault, N., Gardin, S., Locklair, R.E., 2011. Astronomical calibration of the Maastrichtian (Late Cretaceous). *Earth Planet. Sci. Lett.* 305, 328–340.
- Jacobs, L.L., Mateus, O., Polcyn, M.J., Schulp, A.S., Antunes, M.T., Morais, M.L., Tavares, T.D.S., 2006. The occurrence and geological setting of Cretaceous dinosaurs, mosasaurs, plesiosaurs, and turtles from Angola. *J. Paleontol. Soc. Korea* 22, 91–110.
- Jacobs, L.L., Mateus, O., Polcyn, M.J., Schulp, A.S., Scotese, C.R., Goswami, A., Ferguson, K.M., Robbins, J.A., Vineyard, D.P., Neto, A.B., 2009. Cretaceous paleogeography, paleoclimatology, and amniote biogeography of the low and mid-latitude South Atlantic Ocean. *Bull. Geol. Soc. France* 180 (4), 333–341.
- Jacobs, L.L., Strganac, C., Scotese, C.R., 2011. Plate motions, Gondwana dinosaurs, Noah's Arks, Ghost Ships, and Beached Viking Funeral Ships. *An. Acad. Bras. Cienc.* 83 (1), 3–22.
- Jagt, J.W.M., 2005. Stratigraphic ranges of mosasaurs in Belgium and the Netherlands (Late Cretaceous) and cephalopod-based correlations with North America. *Neth. J. Geosci.* 84 (3), 283–301.
- Jarvis, I., Gale, A.S., Jenkyns, H.C., Pearce, M.A., 2006. Secular variation in Late Cretaceous carbon isotopes: a new $\delta^{13}\text{C}$ carbonate reference curve for the Cenomanian–Campanian (99.6–70.6 Ma). *Geol. Mag.* 143, 561–608.
- Jenkyns, H.C., Gale, A.S., Corfield, R.M., 1994. Carbon- and oxygen-isotope stratigraphy of the English Chalk and Italian Scaglia and its palaeoclimatic significance. *Geol. Mag.* 131, 1–34.
- Kiernan, C.R., 2002. Stratigraphic distribution and habitat segregation of mosasaurs in the Upper Cretaceous of western and central Alabama, with an historical review of Alabama mosasaur discoveries. *J. Vertebr. Paleontol.* 22 (1), 91–103.
- Kirschvink, J.L., 1980. The least-squares line and plane and the analysis of palaeomagnetic data. *Geophys. J. Roy. Astron. Soc.* 62, 699–718.
- Li, L., Keller, G., 1999. Variability in Late Cretaceous climate and deep waters: evidence from stable isotopes. *Mar. Geol.* 161, 171–190.
- Marzoli, A., Melluso, L., Morra, V., Renne, P.R., Sgrosso, I., D'Antonio, M., Duarte Morais, L., Morais, E.A.A., Ricci, G., 1999. Geochronology and petrology of Cretaceous basaltic magmatism in the Kwanza basin (western Angola), and relationships with the Paraná–Etendeka continental flood basalt province. *J. Geodyn.* 28, 341–356.
- Mateus, O., Polcyn, M.J., Jacobs, L.L., Araújo, R., Schulp, A.S., Marinheiro, J., Pereira, B., Vineyard, D., 2012. Cretaceous amniotes from Angola: dinosaurs, pterosaurs, mosasaurs, plesiosaurs, and turtles. *Jornadas Internacionais sobre Paleontologia de Dinosaurios y su Entorno*, 75–105.
- Mulder, E.W.A., Formanoy, P., Gallagher, W.B., Jagt, J.W.M., Schulp, A.S., 2013. The first North American record of *Carinodens belgicus* (Squamata, Mosasauridae) and correlation with the youngest in situ examples from the Maastrichtian type area: palaeoecological implications. In: Mulder, E.W.A., Jagt, J.W.M., Schulp, A.S. (Eds.), *The Sunday's Child of Dutch Earth Sciences – A Tribute to Bert Boekschoten on the Occasion of his 80th Birthday*. Netherlands Journal of Geosciences, vol. 92, pp. 145–152.
- Ogg, J.G., Hinnov, L.A., 2012. Cretaceous. In: Gradstein, F.M., Ogg, J.G., Schmidt, M.D., Ogg, G.M. (Eds.), *The Geologic Time Scale 2012*, vol. 2, pp. 793–853 (Chapter 27).
- Polcyn, M.J., Jacobs, L.L., Schulp, A.S., Mateus, O., 2010. The North African mosasaur *Globidens phosphaticus* from the Maastrichtian of Angola. *Hist. Biol.* 22, 175–185.
- Polcyn, M.J., Jacobs, L.L., Schulp, A.S., Mateus, O., 2013. Physical drivers of mosasaur evolution. *Palaeogeogr. Palaeoclimatol. Palaeoecol.* <http://dx.doi.org/10.1016/j.palaeo.2013.05.018>.
- Renne, P.R., Swisher, C.C., Deino, A.L., Karner, D.B., Owens, T., DePaolo, D.J., 1998. Intercalibration of standards, absolute ages and uncertainties in $^{40}\text{Ar}/^{39}\text{Ar}$ dating. *Chem. Geol.* 145, 117–152.
- Schlanger, S.O., Jenkyns, H.C., 1976. Cretaceous Oceanic Anoxic Events: causes and consequences. *Geol. Mjnbouw* 55, 179–184.
- Schlanger, S.O., Arthur, M.A., Jenkyns, H.C., Scholle, P.A., 1987. The Cenomanian–Turonian Oceanic Anoxic Event, I. Stratigraphy and distribution of organic carbon-rich beds and the marine $\delta^{13}\text{C}$ excursion. In: Brooks, J., Fleet, A.J. (Eds.), *Marine Petroleum Source Rocks*, Geological Society London, Special Publication 26, pp. 371–399.
- Scholle, R.A., Arthur, M.A., 1980. Carbon isotope fluctuations in Cretaceous pelagic limestones: potential stratigraphic and petroleum exploration tool. *Am. Assoc. Pet. Geol. Bull.* 64, 67–87.
- Schulp, A.S., Polcyn, M.J., Mateus, O., Jacobs, L.L., Morais, M.L., Tavares, T. da S., 2006. New mosasaur material from the Maastrichtian of Angola, with notes on the phylogeny, distribution and paleoecology of the genus *Prognathodon*. In: Schulp, A.S. (Ed.), *On Maastricht Mosasaurs, Publicaties van het Natuurhistorisch Genootschap in Limburg* 45, pp. 57–67.
- Schulp, A.S., Polcyn, M.J., Mateus, O., Jacobs, L.L., Morais, M.L., 2008. A new species of *Prognathodon* (Squamata, Mosasauridae) from the Maastrichtian of Angola, and the affinities of the mosasaur genus *Liodon*. In: Everhart, M.J. (Ed.), *Proceedings of the Second Mosasaur Meeting*, Fort Hays Studies Special Issue 3. Fort Hays State University, Hays, Kansas, pp. 1–12.
- Schulp, A.S., Polcyn, M.J., Mateus, O., Jacobs, L.L., 2013. Two rare mosasaurs from the Maastrichtian of Angola and the Netherlands. *Neth. J. Geosci.* 92 (1), 3–10.
- Steiger, R.H., Jäger, E., 1977. Subcommittee on geochronology: convention on the use of decay constants in geo- and cosmo-chronology. *Earth Planet. Sci. Lett.* 36, 359–363.
- Thibault, N., Harlou, R., Schovsbo, N., Schiøler, P., Minoletti, F., Galbrun, B., Lauridsen, B.W., Sheldon, E., Stemmerik, L., Surlyk, F., 2012a. Upper Campanian–Maastrichtian nannofossil biostratigraphy and high-resolution carbon-isotope stratigraphy of the Danish Basin: towards a standard $\delta^{13}\text{C}$ curve for the Boreal Realm. *Cretac. Res.* 33, 72–90.
- Thibault, N., Husson, D., Harlou, R., Gardin, S., Galbrun, B., Huret, E., Minoletti, F., 2012b. Astronomical calibration of upper Campanian–Maastrichtian carbon isotope events and calcareous plankton biostratigraphy in the Indian Ocean (ODP Hole 762C): Implication for the age of the Campanian–Maastrichtian boundary. *Palaeogeogr. Palaeoclimatol. Palaeoecol.* 337–338, 52–71.
- Torsvik, T.H., Rouse, S., Labails, C., Smethurst, M.A., 2009. A new scheme for the opening of the South Atlantic Ocean and the dissection of an Aptian salt basin. *Geophys. J. Int.* 177, 1315–1333.
- Voigt, S., Friedrich, O., Norris, R.D., Schönfeld, J., 2010. Campanian–Maastrichtian carbon isotope stratigraphy: shelf-ocean correlation between European shelf sea and the tropical Pacific Ocean. *Newsl. Stratigr.* 44 (1), 57–72.
- Voigt, S., Gale, S.G., Jung, C., Jenkyns, H.C., 2012. Global correlation of Upper Campanian–Maastrichtian successions using carbon-isotope stratigraphy: development of a new Maastrichtian timescale. *Newsl. Stratigr.* 45 (1), 25–53.
- Wagreich, M., 2012. “OAE 3” – regional Atlantic organic carbon burial during the Coniacian–Santonian. *Clim. Past* 8, 1447–1455.